Aalborg Universitet

AALBORG UNIVERSITY

Energy Management System for an Islanded Microgrid with Convex Relaxation

Zia, Muhammad Fahad; Elbouchikhi, Elhoussin; Benbouzid, Mohamed; Guerrero, J. M.

Published in:
IEEE Transactions on Industry Applications

DOI (link to publication from Publisher):
10.1109/TIA.2019.2917357

Publication date:
2019

Document Version
Accepted author manuscript, peer reviewed version

Link to publication from Aalborg University

Citation for published version (APA):
Zia, M. F., Elbouchikhi, E., Benbouzid, M., & Guerrero, J. M. (2019). Energy Management System for an Islanded Microgrid with Convex Relaxation. *IEEE Transactions on Industry Applications*, *55*(6), 7175-7185. Article 8716558. https://doi.org/10.1109/TIA.2019.2917357

General rights
Copyright and moral rights for the publications made accessible in the public portal are retained by the authors and/or other copyright owners and it is a condition of accessing publications that users recognise and abide by the legal requirements associated with these rights.

- Users may download and print one copy of any publication from the public portal for the purpose of private study or research.
- You may not further distribute the material or use it for any profit-making activity or commercial gain
- You may freely distribute the URL identifying the publication in the public portal -

Take down policy
If you believe that this document breaches copyright please contact us at vbn@aub.aau.dk providing details, and we will remove access to the work immediately and investigate your claim.

Downloaded from vbn.aau.dk on: December 06, 2025

This article has been accepted for publication in a future issue of this journal, but has not been fully edited. Content may change prior to final publication. Citation information: DOI 10.1109/TIA.2019.2917357, IEEE Transactions on Industry Applications

Energy Management System for an Islanded Microgrid with Convex Relaxation

Muhammad Fahad Zia, *Student Member*, *IEEE*, Elhoussin Elbouchikhi, *Senior Member*, *IEEE*, Mohamed Benbouzid, *Senior Member*, *IEEE*, Josep M. Guerrero, *Fellow*, *IEEE*

***Abstract*—Conventional generation sources mainly provide energy supply to remote areas nowadays. However, due to growing concerns over greenhouse gas emissions, integration of renewable energy sources is mandatory to meet power demand and reduce climatic effects. The advancements in renewable generation sources and battery storage systems pave the way for microgrids. Microgrids are becoming a viable solution for power supply shortage problems in remote area applications, such as oceanic islands. In this paper, an islanded microgrid, which consists of PV system, tidal turbine, diesel generator, and Li-ion battery, is considered for Ouessant island in Brittany region in France. The economic operation of the microgrid is achieved by including battery degradation cost, levelized costs of energy of PV system and tidal turbine, operating and emission costs of diesel generator, and network constraints. The developed model leads to a non-linear and non-convex problem, which unfortunately can converge to a local optimum solution. The problem has therefore been relaxed and converted to a convex second–order cone model to achieve an optimal decision strategy for islanded microgrid operation with a global or near-global solution. Numerical simulations are carried out to prove the effectiveness of the proposed strategy in reducing the operating and emission costs of the islanded microgrid. It is shown that the developed convex EMS formulation has an optimality gap of less than 1% with reduced computational cost.**

***Index Terms*—Microgrid, island, energy management system, tidal turbine, PV system, demand response, second-order cone programming, convex optimization.**

I. Introduction

Renewable energy sources (RESs) have gained attention of industrialists, scientists, and environmentalists due to exponential rise in global energy demand and drastic climatic effects with increased greenhouse gas (GHG) emissions. The advancement and maturity in RESs technologies have paved the way for their large scale deployment to meet the goals of Paris climate agreement. However, RESs have volatility and intermittent problems, which can be resolved by integrating them with energy storage systems and small scale conventional generation sources. This integration arises energy scheduling and control problems of these distributed energy sources. Microgrid (MG), a low-voltage network, provides the solution to these problems with an ability to operate in both grid-connected and standalone modes [1]–[3].

Numerous islands and other remote areas have no access to utility grid due to high investment cost in transmission system. Therefore, local demand is partially supplied by conventional generation sources, mainly diesel generators (DGs) [4]. However, continuous availability of diesel fuel and high greenhouse gas emissions of these DGs are big problems for these remote areas. Fortunately, RESs, such as solar, wind, and tidal energy (TE) sources, can be used to meet local energy demand and solve these problems.

Marine RESs can play a vital role in meeting electricity demand of the island occupants. Marine RESs consist of ocean thermal energy, ocean osmosis energy, TE, and wave energy sources. The global ocean energy potential is expected to be more than 300 GW in installed capacity by 2050 [5]. TE has currently huge potential among these marine RESs due to relatively marture turbine technologies and higher accuracy in tidal speed prediction.

The gravitational motion of the moon and the sun makes periodic oscillation of the sea level, called tide in the literature. It has the same convectional properties of wave, like amplitude and wavelength. The TE potential is around 75 GW worldwide and 11 GW in Europe. In Europe, UK and France are leading with TE potential of 6 and 3.4 GW, respectively [6]. Worlds' first tidal power station of 240 MW is also located on La Rance river in Brittany. Tidal industry is expanding with more than 100 companies working on it worldwide. The EU accounts for more than 50% of the tidal developers [7].

TE can be harnessed by mainly two methods; tidal barrage and tidal turbines. In tidal barrage, generator produces electric energy due to turbine movements with water flow, which is controlled by opening and closing barrage sluices with the rise and fall of tidal level. It is being used in tidal power stations at Sihwa Lake in South-Korea and La Rance in France. However, tidal barrages lacks promising developments in the future due to limited potential sites, immense capital investment, and negative effects on marine environment [8]. Contrarily, tidal turbines (TTs) have gained huge attention worldwide as they require lesser capital investment for large energy extraction. TTs lead in technology maturity among other marine energy technologies, which is obvious from its technology readiness level [9].

In Europe, Brittany region in France is among the huge TE potential regions. Local energy demand of islands in Brittany region, such as Ouessant island, can be met by using TTs

M. F. Zia and M. E. H. Benbouzid are with the University of Brest, UMR CNRS 6027 IRDL, 29238 Brest, France (e-mail: muhammadfahad.zia@univ-brest.fr; mohamed.benbouzid@univ- brest.fr). M.E.H. Benbouzid is also with the Shanghai Maritime University, 201306 Shanghai, China.
E. Elbouchikhi is with ISEN Yncréa Ouest, UMR CNRS 6027 IRDL, 29200 Brest, France (e-mail: elhoussin.elbouchikhi@isen-ouest.yncrea.fr).
J. M. Guerrero is with the Department of Energy Technology, Aalborg University, 9220 Aalborg, Denmark (e-mail: joz@et.aau.dk).

0093-9994 (c) 2019 IEEE. Personal use is permitted, but republication/redistribution requires IEEE permission. See http://www.ieee.org/publications_standards/publications/rights/index.html for more information.

This article has been accepted for publication in a future issue of this journal, but has not been fully edited. Content may change prior to final publication. Citation information: DOI 10.1109/TIA.2019.2917357, IEEE Transactions on Industry Applications

along with other energy sources. Hence, MG system sizing was performed in [10]. Authors have achieved the optimal sizing of a hybrid power generation system. It comprises PV system, TT, wind turbine, and battery storage system. In [11], wind, tidal, and pumped hydro storage-based MG system was proposed and designed to reduce GHG emissions. However, the industrial proposal for Ouessant island include diesel generator, PV system, TT, and Li-ion battery system. Therefore, an islanded MG, which consists of PV system, TT, DG, and Li-ion battery, has been designed to meet the electricity demand of the island. In this regard, we proposed an islanded marine MG system for Ouessant island in [12]. An EMS was developed to minimize the MG system operating cost. However, the developed EMS is non-convex. Morevoer, it does not include DG GHG emissions and demand response (DR) in MG operation.

Islanded MG requires energy management system (EMS) to optimize its daily energy scheduling operation [13]. An EMS receives energy generation and load demand information from all local sources, and determines decision strategies for each local source by performing optimization on various objectives [1]. Various EMS approaches have already been proposed in the literature. In [14], optimal EMS was developed for PV and fuel cell-based MG to minimize its operating cost. A linear programming (LP) EMS was developed for grid-connected MG with tidal generation and pumped hydro storage system in [15]. In [16], authors developed LP and mixed integer linear programming (MILP) based EMS models. MILP-based MG EMSs were developed and experimentally validated in [17], [18]. In [19], authors developed a MILP model for optimal dispatch of PV and storage-based MG. Another MILP model is presented in [20] for residential MG EMS by applying Taylor series approximation, estimation operation points, and auxiliary variables-based methods on the original non-linear problem. The developed model had achieved solution error below 2% with lesser computations. Authors in [21] proposed operating and emission costs-based mixed integer quadratic EMS model for isolated MG and they also studied DR impacts on MG operation. In [22], authors presented a mixed integer nonlinear programming (MINLP) model to incorporate DR into MG EMS. It achieved the objective of minimizing operating cost of DGs and penalty cost on energy curtailment with higher computations. A mixed integer second-order cone programming (MISOCP) based EMS model was developed in [23], which minimizes load shedding cost of isolated MG. However, integer variables increases computations and causes convergence problems. Moreover, they lack in providing solutions against TT-based islanded MG EMS, battery degradation cost consideration, and DR computations at each bus.

In this context, this work aims at developing integer-free second-order cone programming-based EMS (SOCP-EMS) model to minimize operating and emission costs of islanded MG. The proposed model includes operating and emission cost of DG, levelized costs of energy (LCOEs) of TT and PV system, battery degradation cost, generation sources and battery operational constraints, incentive-based DR model, and AC power flow; and guarantees global optimality. To the best knowledge of the authors, no SOCP-EMS model with these characteristics has been proposed for MGs [1], [24].

The main contributions of this work are as follows:

- Optimal EMS model is proposed to enable effective integration of RESs, DG, and local energy storage into islanded MG.
- TT integration and modeling in islanded MG EMS is included.
- An incentive-based DR scheme is introduced for active participation of consumers.
- Convex-SOCP model is proposed for the developed non-convex EMS problem.
- Integer-free EMS model substantially reduces computations; thus paving the way for real-time implementation in MGs.

The rest of the paper is organized as follows. Section II presents islanded MG architecture and models its components. Section III develops a non-linear EMS optimization problem. Section IV converts the proposed non-convex EMS problem into relaxed convex SOCP model. Section V presents the simulation setup and results. Finally, conclusion is presented in Section VI.

II. Islanded Microgrid Model

Ouessant island, (48°28′N, 5°5′W), is considered as a case study for islanded marine MG. It is located in Brittany region in France with a total population of 862 inhabitants. It has huge tidal energy potential in Fromveur strait [25], [26], and electric power can be produced up to 500 MW [27].

A. System Architecture

The marine MG system is the most suitable power system for islands with marine energy potential. Therefore, an islanded marine MG system is proposed in Fig. 1. It consists of PV system, TT, DG, Li-ion battery, and power converters. It also includes an island power network to consider system losses and buses voltages. The power demand is divided into two categories, namely critical and responsive loads (RLs). The RLs are used for DR operation in MG energy scheduling. MG requires local controllers (LCs) and MG central controller (MGCC) to share information and data using efficient communication technologies. The communication technologies are mainly selected on the basis of coverage area, data rate, and

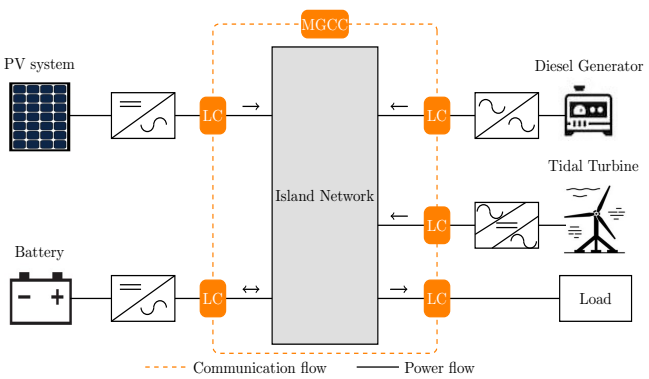

Fig. 1. Islanded AC MG architecture.

0093-9994 (c) 2019 IEEE. Personal use is permitted, but republication/redistribution requires IEEE permission. See http://www.ieee.org/publications_standards/publications/rights/index.html for more information.

This article has been accepted for publication in a future issue of this journal, but has not been fully edited. Content may change prior to final publication. Citation information: DOI 10.1109/TIA.2019.2917357, IEEE Transactions on Industry Applications

deployment cost [1]. Wireless communication technologies are better options for marine MG systems at islands. LCs and MGCC share information to optimize the MG EMS operation.

B. Diesel Generator

DGs are the only major energy sources in islands. They often partially meet the energy demand. They operate with RESs to provide continuous power supply to load ends. DGs have higher operating costs in islands due to high transportation cost. The operating cost model of DG is [11]:

$$OC_t^g = a(P_t^g)^2 + aP_t^g + c, \quad t \in \mathcal{T} \tag{1}$$

where a, b and, c are DG cost coefficients. P_t^g is DG scheduled output power at time t.

DGs have higher GHG emissions that adversely affect the global climate. Therefore, the emission cost of DG is modeled in (2).

$$EC_t^g = \pi^e E^g P_t^g, \quad t \in \mathcal{T} \tag{2}$$

DG emission cost includes the equivalent lifecycle carbon emissions, E^g, and penalty cost on them, π^e, to achieve environmental sustainability objective.

C. Tidal Turbine

TTs convert the kinetic energy of tidal stream into electric energy. TTs are installed below the water, thus creating an obstruction at seas surface level. TTs are mainly categorized into horizontal-axis, vertical-axis, duct type, oscillating hydrofoil TTs, and tidal kites [28], [29]. In [30], critical analysis on different TTs drivetrain options was presented to compare their performances, which helps in selecting TTs for marine energy conversion systems.

Tidal speed can be calculated by (3) using spring tidal speed, $\upsilon_{sm,t}$, and neap tidal speed, $\upsilon_{nm,t}$, information at the reference location.

$$\upsilon_{m,t} = \upsilon_{nm,t} + \frac{(C - \gamma_{nm})(\upsilon_{sm,t} - \upsilon_{nm,t})}{\gamma_{sm} - \gamma_{nm}} \tag{3}$$

where C is the tidal coefficient, which estimates the amplitude of tides forecasts. γ_{sm} and γ_{nm} are the tidal coefficients of the spring and neap tides, respectively.

The TT output power depends on turbine swept area, turbine power coefficient, and tidal speed. The estimated output power, $P_{a,t}^m$, is determined using (4). TT cannot produce power below cut-in tidal speed, υ_{ci}. The output power increases with tidal speed until it reaches its maximum power at rated tidal speed, υ_r. It produces maximum power above rated tidal speed. However, it stops producing electric power after cut-out tidal speed, υ_{co}, to avoid TT structural damage.

$$P_{a,t}^m = \begin{cases} 0, & \upsilon_t < \upsilon_{ci} \\ \frac{1}{2}\rho\wp^m\pi R^2\upsilon_t^3, & \upsilon_{ci} \le \upsilon_t < \upsilon_r \\ \frac{1}{2}\rho\wp^m\pi R^2\upsilon_r^3, & \upsilon_r \le \upsilon_t \le \upsilon_{co} \\ 0, & \upsilon_t > \upsilon_{co} \end{cases} \quad t \in \mathcal{T} \tag{4}$$

where ρ is water density. $\wp^m$ and πR^2 are TT power coefficient and swept area, respectively. The TT operational cost is modeled as:

$$OC_t^m = C^m P_t^m, \quad t \in \mathcal{T} \tag{5}$$

LCOE criteria is used to determine TT electricity production cost, C^m, in (6). It comprises investment cost, C_{inv}^m (€), operation and maintenance costs, C_{om}^m (€/year), annual energy output, E_{an}^m, discount rate dr, and TT degradation factor, σ^m.

$$C^m = \frac{C_{inv}^m + \sum_{i=1}^n C_{om}^m (1+dr)^{-i}}{\sum_{i=1}^n E_{an}^m (1-\sigma^m)^{i-1}(1+dr)^{-i}} \tag{6}$$

The discount rate, dr, is used to compute yearly present values of C_{om}^m and E_{an}^m over system lifetime of n years. σ^m accounts the degradation in TT annual energy output after first year. σ^m accounts bio-fouling, salts-induced material corrosion, marine creatures, flotsam, and blade cavitation effects in TTs degradation [31].

D. PV System

The available output power of PV system denoted $P_{a,t}^s$ is given by (7) [32]. It computes the PV power using solar irradiance, G_t, and temperature, T_t, data at each time t.

$$P_{a,t}^s = N^s P_{STC}^s \left[\frac{G_t}{G_{STC}} (1 - \gamma(T_{c,t} - T_{STC})) \right], \; t \in \mathcal{T} \tag{7}$$

where N^s is the number of PV arrays. G_{STC}, T_{STC}, and P_{STC}^s, are irradiance, temperature, and PV array output power at standard test conditions. γ is the temperature-dependent degradation coefficient. $T_{c,t}$ is PV cell temperature, and it is computed as:

$$T_{c,t} = T_t + \frac{G_t}{G_{NOCT}} (NOCT - 20), \quad t \in \mathcal{T} \tag{8}$$

where G_{NOCT} is irradiance at nominal operating cell temperature.

The operational cost of PV system, OC_t^s, is provided by:

$$OC_t^s = C^s P_t^s, \quad t \in \mathcal{T} \tag{9}$$

where C^s is the LCOE of PV system in €$/kWh$, and it is modeled in (10).

$$C^s = \frac{C_{inv}^s + \sum_{i=1}^n C_{om}^s (1+dr)^{-i}}{\sum_{i=1}^n E_{an}^s (1-\sigma^s)^{i-1}(1+dr)^{-i}} \tag{10}$$

The LCOE model of PV system includes investment cost, C_{inv}^s, operation and maintenance costs, C_{om}^s, annual energy output, E_s^m, discount rate dr, and PV system degradation factor, σ^s. The discount rate is used to compute yearly present values of C_{om}^s and E_{an}^s over system lifetime of n years. σ^s accounts the degradation in PV annual energy output after first year.

E. Battery

Li-ion battery has gained huge attention among other batteries due to its high energy density and technology maturity. Let OC_t^b and C_t^b denote the battery operational and degradation

0093-9994 (c) 2019 IEEE. Personal use is permitted, but republication/redistribution requires IEEE permission. See http://www.ieee.org/publications_standards/publications/rights/index.html for more information.

This article has been accepted for publication in a future issue of this journal, but has not been fully edited. Content may change prior to final publication. Citation information: DOI 10.1109/TIA.2019.2917357, IEEE Transactions on Industry Applications

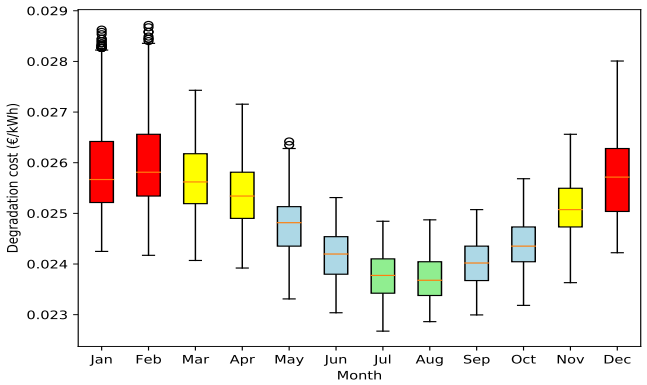

Fig. 2. Battery degradation cost variation at 50% DOD.

costs at time t, respectively. The battery operational cost with charging, η^{b+}, and discharging efficiencies, η^{b-}, is modeled as:

$$OC_t^b = C_t^b \left(\eta^{b+} P_t^{b+} + \frac{P_t^{b-}}{\eta^{b-}} \right), \quad t \in \mathcal{T} \tag{11}$$

where P_t^{b+} and P_t^{b-} are battery charging and discharging powers at time t, respectively.

The degradation cost model includes depth of discharge (DOD) and temperature-dependent capacity and power fading effects of battery. The degradation cost is calculated as [32]:

$$C^b = \frac{1}{2} \frac{\left[C_{inv}^b + \sum_{i=1}^{n} C_{om}^b (1+dr)^{-i} \right] (1+dr)^n - SV}{(1+dr)^n \chi_T^E \chi_T^{\Upsilon} \chi_d^{\Upsilon} \Upsilon_r^b E_r^b} \tag{12}$$

where χ_T^E is normalized temperature-dependent power fading coefficient. χ_T^{Υ} and χ_d^{Υ} are temperature and DOD-dependent capacity fading coefficients. The regression modeling of these coefficients are detailed in [32]. Υ_r^b and E_r^b are rated cyclelife and energy capacity of battery. Salvage value (SV) is the value of battery at the end of its useful life.

The charge (discharge) rates control the charging (discharging) power of battery, which are defined as:

$$P_t^{b+} = l_t^+ E_r^b, \quad t \in \mathcal{T} \tag{13}$$

$$P_t^{b-} = l_t^- E_r^b, \quad t \in \mathcal{T} \tag{14}$$

where l_t^+ and l_t^- are battery charge and discharge rates, respectively.

The degradation cost variation in each month is shown as boxplot in Fig. 2 for Ouessant island. It is low in the months of July and August, while higher in December, January, and February for fixed DOD ($d = 0.5$). Hence, battery operational cost will be higher in winter due to low temperature.

F. Demand Response

MG operator offers incentives to consumers against the control of RLs shifting. The operator receives the RLs data, which includes their proportion of total load and set of shifting instants, $\mathcal{T}_s$. The shifting instants can be forward, backward, or both. RLs, $D^r = D^{pr} + jD^{qr}$, are deferred to the scheduled ones and consumers will get the incentives in return. D^{pr} and D^{qr} are RLs active and reactive components, respectively. Equation (15) defines the shifting of RLs active power from instant t to i, while their recovering is modeled in (16).

$$D_{x,t}^{pr+} = \sum_{\substack{i \in \mathcal{T}_s \\ i \neq t}} D_{x,t,i}^{pr}, \quad x \in \mathcal{N}_{\mathcal{X}}, t \in \mathcal{T} \tag{15}$$

$$D_{x,t}^{pr-} = \sum_{\substack{i \in \mathcal{T}_s \\ i \neq t}} D_{x,i,t}^{pr}, \quad x \in \mathcal{N}_{\mathcal{X}}, t \in \mathcal{T} \tag{16}$$

where $D_{x,t}^{pr+}$ and $D_{x,t}^{pr-}$ are RL shifted and recovered active powers at load bus x and time t, respectively. RL active and reactive powers are strongly correlated: if RL active power is increased or decreased, its reactive power will do the same. Therefore, it is assumed that RL active and reactive power can be related with one reasonable method: RL power factor remains constant, which means that $D_{x,t}^{qr} = D_{x,t}^{pr} \tan \phi_x$, and ϕ_x is RL power factor angle at bus x.

The incentive cost for MG operator is:

$$IC_t^r = \sum_{x \in \mathcal{N}_{\mathcal{X}}} \beta^r D_{x,t}^{pr+}, \quad t \in \mathcal{T} \tag{17}$$

where β^r corresponds to the fixed incentive rate for consumers against RLs shifting.

G. Network Model

Consider an islanded MG consisting of $\mathcal{N}$ buses. Active power, $P_{i,t}$ and reactive power, $Q_{i,t}$, are the difference of generation and load, critical and responsive loads, at each bus i and time t. The network model is incorporated into MG EMS to achieve its operation within the operating voltage limits and system losses restriction. The power flow equation of the network model are:

$$P_{i,t} = \sum_{\substack{j=1 \\ j \neq i}}^{\mathcal{N}} \Re \left\{ \underline{V}_{i,t} (\underline{V}_{i,t}^* - \underline{V}_{j,t}^*) y_{ij}^* \right\}, \ i,j \in \mathcal{N}, t \in \mathcal{T} \tag{18}$$

$$Q_{i,t} = \sum_{\substack{j=1 \\ j \neq i}}^{\mathcal{N}} \Im \left\{ \underline{V}_{i,t} (\underline{V}_{i,t}^* - \underline{V}_{j,t}^*) y_{ij}^* \right\} \ i,j \in \mathcal{N}, t \in \mathcal{T} \tag{19}$$

where $\underline{V}_{i,t}$ is the complex voltage of bus i at time t. y_{ij} is the branch admittance between buses i and j, and $y_{ij} = \frac{1}{r_{ij} + j x_{ij}}$. r_{ij} and x_{ij} are the branch resistance and reactance between buses i and j, respectively.

III. Energy Management Model

Consider an islanded MG of $\mathcal{N}$-bus system. The EMS model is developed to optimize MG operation over a scheduling horizon $\mathcal{T} := \{t_s, t_s + \Delta t, t_s + 2\Delta t, ..., t_f\}$. The model aims to minimize the islanded MG operating and emission costs, which comprises DG operating and emission costs, LCOEs of PV system and TT, battery degradation cost, and DR incentive cost. The cost relations of RESs and battery storage systems comprises investment cost, operation and

0093-9994 (c) 2019 IEEE. Personal use is permitted, but republication/redistribution requires IEEE permission. See http://www.ieee.org/publications_standards/publications/rights/index.html for more information.

This article has been accepted for publication in a future issue of this journal, but has not been fully edited. Content may change prior to final publication. Citation information: DOI 10.1109/TIA.2019.2917357, IEEE Transactions on Industry Applications

maintenance cost, and degradation parameters. The details of the proposed model are in the following:

$$\min \quad \sum_{t\in\mathcal{T}} \{OC_t^g + EC_t^g + OC_t^m + OC_t^s + OC_t^b + IC_t^r\}\,\Delta t \tag{20a}$$

s.t. (1), (2), (6), (11), (13), (15)–(21)

$$P_{min}^g \le P_t^g \le P_{max}^g, \quad t\in\mathcal{T} \tag{20b}$$

$$Q_{min}^g \le Q_t^g \le Q_{max}^g, \quad t\in\mathcal{T} \tag{20c}$$

$$0 \le P_t^m \le P_{a,t}^m, \quad t\in\mathcal{T} \tag{20d}$$

$$0 \le P_t^s \le P_{a,t}^s, \quad t\in\mathcal{T} \tag{20e}$$

$$(P_t^m)^2 + (Q_t^m)^2 \le (S^m)^2, \quad t\in\mathcal{T} \tag{20f}$$

$$(P_t^s)^2 + (Q_t^s)^2 \le (S^s)^2, \quad t\in\mathcal{T} \tag{20g}$$

$$0 \le l_t^+ \le l_{max}^+, \quad t\in\mathcal{T} \tag{20h}$$

$$0 \le l_t^- \le l_{max}^+, \quad t\in\mathcal{T} \tag{20i}$$

$$l_t^+ l_t^- = 0, \quad t\in\mathcal{T} \tag{20j}$$

$$E_t^b = E_{t-1}^b + \left[\eta^+ P_t^{b+} - \frac{P_t^{b-}}{\eta^-}\right]\Delta t,\ t\in\mathcal{T} \tag{20k}$$

$$E_{t_f}^b = E_{t_s}^b \tag{20l}$$

$$E_{max}^b = E_r^b \chi_{\mu_T}^{\Xi} \tag{20m}$$

$$E_{min}^b = E_{max}^b(1-d) \tag{20n}$$

$$E_{min}^b \le E_t^b \le E_{max}^b \tag{20o}$$

$$(P_t^{b+} - P_t^{b-})^2 + (Q_t^b)^2 \le (S^b)^2, \quad t\in\mathcal{T} \tag{20p}$$

$$D_{x,t}^{pr+} D_{x,t}^{pr-} = 0, \quad x\in\mathcal{N}_{\mathcal{X}}, t\in\mathcal{T} \tag{20q}$$

$$\sum_{t\in\mathcal{T}} D_{x,t}^{pr+} = \sum_{t\in\mathcal{T}} D_{x,t}^{pr-}, \quad x\in\mathcal{N}_{\mathcal{X}} \tag{20r}$$

$$D_{x,t,i}^{pr} \le D_{x,t,max}^{pr}, \quad x\in\mathcal{N}_{\mathcal{X}}, t\in\mathcal{T} \tag{20s}$$

$$D_{x,t}^{pr+} \le D_{x,t,max}^{pr}, \quad x\in\mathcal{N}_{\mathcal{X}}, t\in\mathcal{T} \tag{20t}$$

$$D_{x,t}^{pr+}, D_{x,t}^{pr-} \ge 0, \quad x\in\mathcal{N}_{\mathcal{X}}, t\in\mathcal{T} \tag{20u}$$

$$P_t^g + P_t^m + P_t^s - P_t^{b+} + P_t^{b-} + \sum_{x\in\mathcal{N}_{\mathcal{X}}} \left(D_{x,t}^{pr+} - D_{x,t}^{pr-}\right) \le (1+\alpha) D_t^p, t\in\mathcal{T} \tag{20v}$$

$$V_{i,min} \le V_{i,t} \le V_{i,max}, \quad i\in\mathcal{N}, t\in\mathcal{T} \tag{20w}$$

$$\theta_{ij,min} \le \measuredangle\underline{V}_{i,t} - \measuredangle\underline{V}_{j,t} \le \theta_{ij,max}, \quad i,j\in\mathcal{N}, t\in\mathcal{T} \tag{20x}$$

where $\measuredangle\underline{V}_{i,t}$ is the phase angle of complex voltage $\underline{V}_{i,t}$ at bus i. $\theta_{ij,min}$ and $\theta_{ij,max}$ are the minimum and maximum limits on phase angle difference between buses i and j, respectively.

Constraints (20b) and (20c) define the operational limits on DG active and reactive powers output, respectively. (20d) and (20e) represent the limits on output active power from TT and PV system, respectively. The inverters capabilities of TT and PV system are provided in convex quadratic inequalities (20f) and (20g), respectively [33]–[35]. S_t^m and S_t^s are apparent power ratings of TT and PV inverters, respectively. Constraints (20h) and (20i) ensure that the battery charging and discharging operation remains within the limits of maximum allowable charge (discharge) rates, respectively. Constraint (20j) prohibits battery concurrent charging and discharging operations. The dynamic energy state representation of battery is provided in (20k). Constraint (20l) ensures that battery initial and final energy states remain the same. Constraints (20m)–(20o) represent the limits on battery energy state. Constraint (20p) corresponds to reactive power capability of battery inverter [36]. Constraint (20q) prohibits simultaneous shifting and recovering of RL. Constraint (20r) ensures that the total shifted and recovered RLs are the same. Inequalities (20s) – (20u) represents RL limits. Constraint (20v) stands for limiting total active power losses, with α representing allowable active power losses ratio. Constraints (20w) and (20x) correspond to the limits on bus voltage magnitude and buses phase angle difference, respectively.

IV. Convex Formulation

MG EMS problem (20) is intrinsically non-convex non-linear programming (NLP) model due to battery constraint (20j), DR constraint (20p), and network constraints (18) and (19). It arises local optimality issues. However, these constraints can be relaxed into convex ones [37]. Battery constraints (20h)–(20j) are modified into mixed integer linear equations (21a)–(21c).

$$0 \le l_t^+ \le \delta_t\, l_{max}^+, \quad t\in\mathcal{T} \tag{21a}$$

$$0 \le l_t^- \le (1-\delta_t)\, l_{max}^-, \quad t\in\mathcal{T} \tag{21b}$$

$$\delta_t \in \{0,1\}, \quad t\in\mathcal{T} \tag{21c}$$

where δ_t is a binary variable for battery at instant t. However, these binary variables may cause higher computation burden; thus making solution time more expensive. Therefore, binary constraint (21c) is relaxed into the continuous one (21d).

$$0 \le \delta_t \le 1, \quad t\in\mathcal{T} \tag{21d}$$

DR constraint (20q) is also non-convex and non-linear, which is converted into convex linear constraints (22) by also replacing equations (20t) and (20u).

$$0 \le D_{x,t}^{pr+} \le \xi_{x,t}\, D_{x,t,max}^{pr}, \quad x\in\mathcal{N}_{\mathcal{X}}, t\in\mathcal{T} \tag{22a}$$

$$0 \le D_{x,t}^{pr-} \le (1-\xi_{x,t})\, M, \quad x\in\mathcal{N}_{\mathcal{X}}, t\in\mathcal{T} \tag{22b}$$

$$0 \le \xi_{x,t} \le 1, \quad x\in\mathcal{N}_{\mathcal{W}}, t\in\mathcal{T} \tag{22c}$$

where M is a large number and islanded MG operator can chose it on the basis of peak demand limit. It should not be very large to avoid convergence problems.

MG network power flow constraints (18) and (19) are non-convex due to voltage product component, $\underline{V}_{i,t}\underline{V}_{j,t}^*$. These equations can be convexified using existing methods in the literature [38]–[40]. In this paper, SOCP method is preferred

0093-9994 (c) 2019 IEEE. Personal use is permitted, but republication/redistribution requires IEEE permission. See http://www.ieee.org/publications_standards/publications/rights/index.html for more information.

This article has been accepted for publication in a future issue of this journal, but has not been fully edited. Content may change prior to final publication. Citation information: DOI 10.1109/TIA.2019.2917357, IEEE Transactions on Industry Applications

over semi-definite programming (SDP) for its lower computational complexity [41]. Let $\underline{H}_{ij,t} = \underline{V}_{i,t}\underline{V}^*_{j,t}$, and the constraints (18), (19), (20w), (20x) are transformed into the following [42], [43]:

$$P_{i,t} = \sum_{\substack{j=1 \\ j\neq i}}^{\mathcal{N}} \Re\left\{(\underline{H}_{ii,t} - \underline{H}_{ij,t})y^*_{ij}\right\},\ i,j \in \mathcal{N}, t \in \mathcal{T} \quad (23a)$$

$$Q_{i,t} = \sum_{\substack{j=1 \\ j\neq i}}^{\mathcal{N}} \Im\left\{(\underline{H}_{ii,t} - \underline{H}_{ij,t})y^*_{ij}\right\},\ i,j \in \mathcal{N}, t \in \mathcal{T} \quad (23b)$$

$$V^2_{i,min} \leq H_{ii,t} \leq V^2_{i,max},\ i \in \mathcal{N}, t \in \mathcal{T} \quad (23c)$$

$$\tan(\theta_{ij,min}) \leq \frac{\Im\left\{\underline{H}_{ij,t}\right\}}{\Re\left\{\underline{H}_{ij,t}\right\}} \leq \tan(\theta_{ij,max}),$$
$$i,j \in \mathcal{N}, t \in \mathcal{T} \quad (23d)$$

The non-convexity in $H_{ij,t} = V_{i,t}V^*_{j,t}$ is converted into convex SOC form as:

$$H_{ij,t} \leq H_{ii,t}H_{jj,t}, \quad i,j \in \mathcal{N}, t \in \mathcal{T} \quad (23e)$$

MG non-convex EMS model (20) is transformed into relaxed convex SOCP model as:

$$\min \quad \sum_{t\in\mathcal{T}} \{OC^g_t + EC^g_t + OC^m_t + OC^s_t + OC^b_t + IC^r_t\}\Delta t \quad (24)$$

s.t. (1), (2), (6), (11), (13), (15)–(17), (20b)–(20i), (20b)–(20g), (20k)–(20p), (20r), (20s), (20v), (21a), (21b), (21d), (22), (23)

This relaxed convex SOCP-EMS model can be solved by Gurobi [44], while the non-convex EMS model is solved by IPOPT [45] in GEKKO Python [46]. The relaxed SOCP model solution is feasible and globally optimum, if it satisfies the original non-convex EMS problem constraints.

V. Simulation Setup and Results

The proposed SOCP-EMS is tested on a 7-bus islanded MG, as shown in Fig. 3. It consists of DG at root bus 1, PV system at bus 3, battery at bus 4, and TT at bus 6. buses 2, 4, 5, and 7 are load buses. MG is a low-voltage network, therefore, system voltage is assumed to be 230 V. The network data of the islanded MG are provided in Table I. The line impedances are set following the criteria of $\frac{R}{X}$ ratio to be at least 7.7 in distribution system [47], [48]. The scheduling horizon is considered 24h. Table II presents the technical data of DG, TT, PV, and battery. Maximum charge and discharge rates of battery are bounded by 0.5 each. Salvage value of battery is assumed to be 40% of capital cost. The discount rate is considered 4%. Four cases are considered to study the effectiveness of the proposed EMS model for 24h period. Battery remains operational in all the following cases:

- Case I: All DG, PV, and TT units are online for July.
- Case II: Only PV system is off–line for July.
- Case III: Only TT is off–line for July.
- Case IV: All DG, PV, and TT units remain online for December.

Figures 4 and 5 present the temperature, PV power, TT

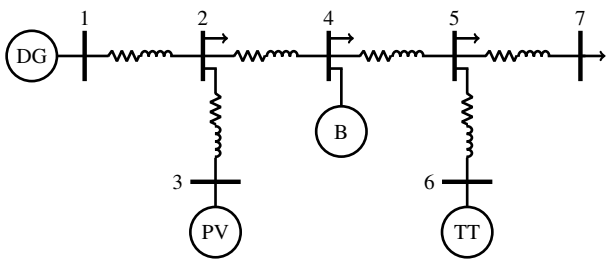

Fig. 3. 7-bus microgrid test network.

TABLE I
7-BUS MICROGRID TEST NETWORK DATA.

Br. no.	Rx. nd.	Sn. nd.	R (Ω)	X (Ω)
1	1	2	0.482	0.062
2	2	3	0.233	0.017
3	2	4	0.416	0.035
4	4	5	0.165	0.021
5	5	6	0.642	0.083
6	5	7	0.416	0.035

TABLE II
TECHNICAL DATA.

Diesel generator					
a, b, c	0.01, 0.5, 0	E^g (g/kWh)	778	π^e (€/kWh)	35
P^g_{min}, P^g_{max} (kW)	0.5, 6	Q^g_{min}, Q^g_{max} (kVAR)	-1, 4		
Tidal turbine					
C^m_{inv} (€/kW)	3500	C^m_{om} (€/kW–year)	140	C^m (€/kWh)	0.232
Rated Power (kW)	3	σ^m (%)	2	S^m (kVA)	3.2
v_{ci} (m/s)	0.5	v_r (m/s)	2.7	v_{co} (m/s)	5
γ_{sm}	95	γ_{nm}	45	R (m)	0.5
PV sytem					
C^s_{inv} (€/kW)	1930	C^s_{om} (€/kW–year)	22	C^s (€/kWh)	0.148
Rated Power (kW)	4	σ^s (%)	0.05	S^s (kVA)	4.3
Li-ion battery					
C^b_{inv} (€/kWh)	200	C^b_{om} (€/kW–year)	20	η^{b+}, η^{b-}	0.9
E^b_r (kWh)	10	d (%)	0.5	S^b (kVA)	5.3

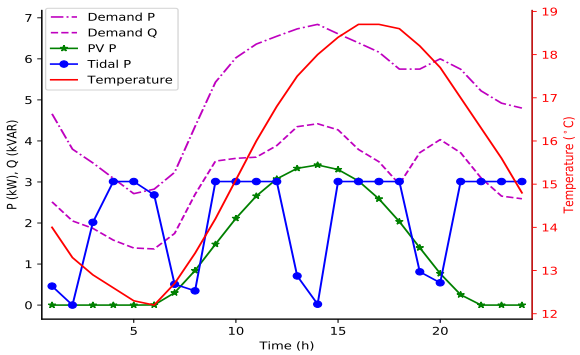

Fig. 4. PV, tidal turbine, load, and temperature data for July.

0093-9994 (c) 2019 IEEE. Personal use is permitted, but republication/redistribution requires IEEE permission. See http://www.ieee.org/publications_standards/publications/rights/index.html for more information.

This article has been accepted for publication in a future issue of this journal, but has not been fully edited. Content may change prior to final publication. Citation information: DOI 10.1109/TIA.2019.2917357, IEEE Transactions on Industry Applications

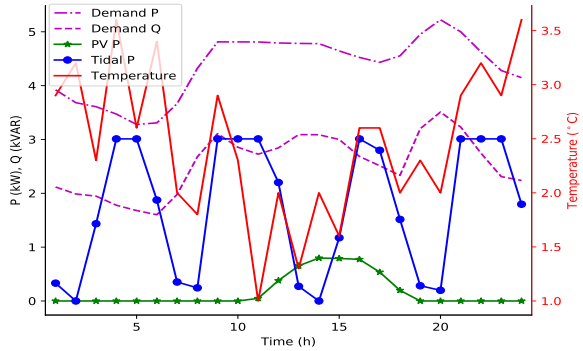

Fig. 5. PV, tidal turbine, load, and temperature data for December.

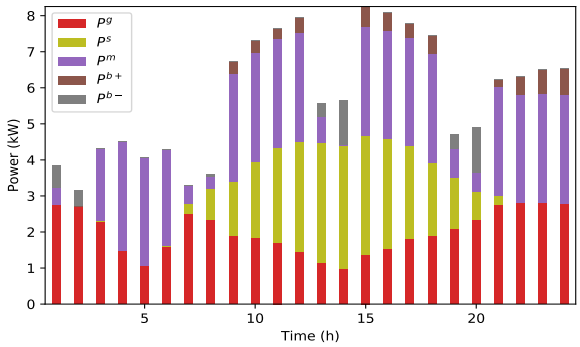

Fig. 6. Islanded microgrid scheduling profile.

power, and demand profiles of Ouessant island for 24h period in July and December, respectively. The active and reactive demands at load buses 2, 4, 5, and 7 are assumed to be 35%, 15%, 25%, and 25% of total demand, respectively. DR power factor for each load bus is considered to be 0.85 for this case study. The fixed DR incentive is assumed to be 15 €/MWh. RL is considered 20% of base active load. Maximum limit on active power losses is considered 5% of the total active demand for the islanded MG network. Bus voltage deviations are limited within $\pm$ 5%. All the simulations are performed on an i5 2.8-GHz processor with 16 GB RAM.

A. SOCP-EMS Performance

The proposed SOCP-EMS is evaluated by measuring optimality gap between the original non-convex EMS and relaxed SOCP-EMS using the following formula:

$$\text{optimality gap} = \frac{\text{original EMS - relaxed EMS}}{\text{original EMS}} \tag{25}$$

The optimality gap is less than 1% for each case, as shown in Table III. Moreover, the SOCP–EMS runtime is far better than that of a non-convex EMS in each case. It proves that the proposed SOCP-EMS model provides a global optimal solution with reduced computation cost. Hence, it can be used in optimizing islanded MG scheduling.

The islanded MG scheduling for each case study is provided in the following:

1) Case I: In this case, all generation and storage units are online. Figure 6 shows the scheduled power profiles of DG, PV, TT, and battery. DG will remain on all the time as RESs and battery cannot meet the load demand. Battery is charging during high TT and PV output power. It discharges to provide supply to load ends when PV system and TT have low or no output power. The active power demands before and after DR are shown in Fig. 7. After DR, load increases to use excess TT output power during $t = 3h$ to $t = 6h$ as demand is minimum during this period. Load decreases at $t = 7h$ and $t = 8h$ due to low availability of PV output power. Then load increases again during high power outputs of both TT and PV system, and decreases at peak demand period.

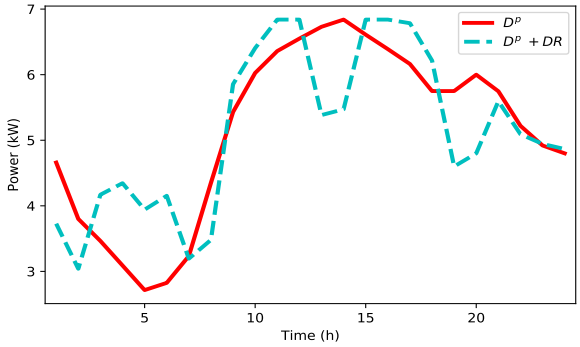

Fig. 7. Active demand with demand response.

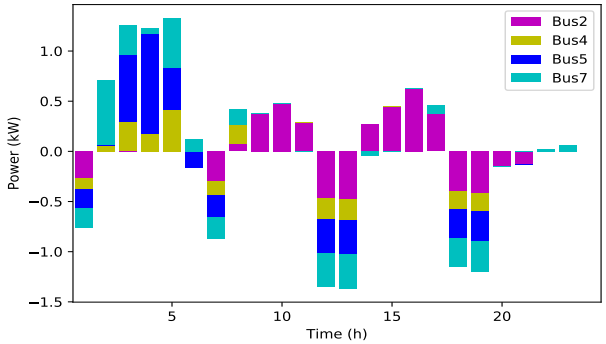

Fig. 8. Demand response profile at load buses.

DR profile at each load bus is presented in Fig. 8. Bus 2 recovers shifted RL at high generation power periods of both PV system and TT, which is shifted from low generation periods. Other load buses shift RL from high demand and low TT output power periods to low demand period. Figure 9 shows the voltage profiles of islanded MG network buses. Bus 1, DG bus, is taken as a root bus, therefore, its voltage will remain the same at 230 V. The variations in buses voltages remain within the specified operational limits of $\pm$ 5%. The active losses of the islanded MG network are shown in Fig. 10. They vary with the load demand. They are higher at high demand periods, but they do not go beyond the specified losses threshold.

TABLE III
SOCP-EMS PERFORMANCE

	Non-convex EMS		SOCP-EMS		
	Obj. value (€)	Runtime (s)	Obj. value (€)	Optimality gap (%)	Runtime (s)
Case-I	41.304	213.2	41.025	0.68	6.23
Case-II	53.901	156.7	53.891	0.02	6.84
Case-III	57.695	124.3	57.254	0.08	7.21
Case-IV	44.713	169.3	44.578	0.30	5.86

0093-9994 (c) 2019 IEEE. Personal use is permitted, but republication/redistribution requires IEEE permission. See http://www.ieee.org/publications_standards/publications/rights/index.html for more information.

This article has been accepted for publication in a future issue of this journal, but has not been fully edited. Content may change prior to final publication. Citation information: DOI 10.1109/TIA.2019.2917357, IEEE Transactions on Industry Applications

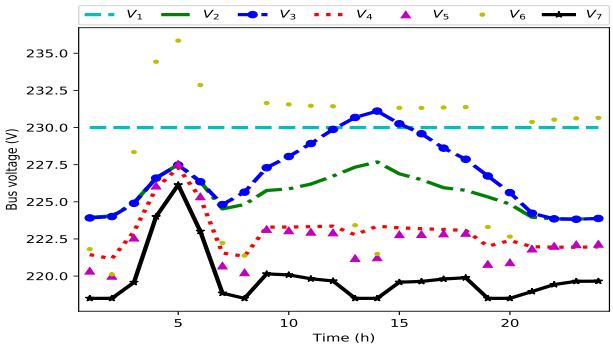

Fig. 9. Buses voltage profile.

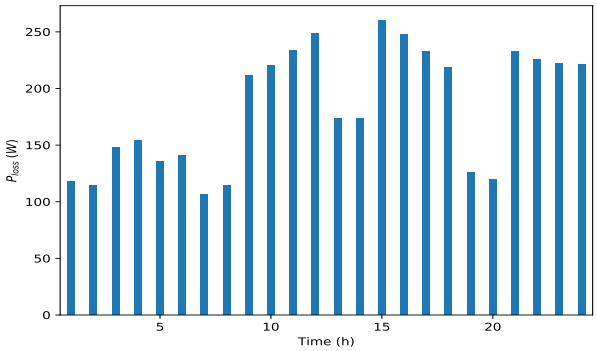

Fig. 10. Active power losses of the islanded microgrid system.

2) Case II: In this case, PV system is considered off–line. The power scheduling profiles of DG, TT and, battery are presented in Fig. 11. TT and battery cannot meet the load demand. Therefore, DG remains on all the time. Battery is discharging at $t = 2h$ to $t = 14h$ when TT does not produce power. Battery is charging during low demand and high TT power periods. Figure 12 shows active power demand profile with and without DR. It clearly shows that DR has shifted responsive load from low to high TT power output periods to avoid DG to produce more power.

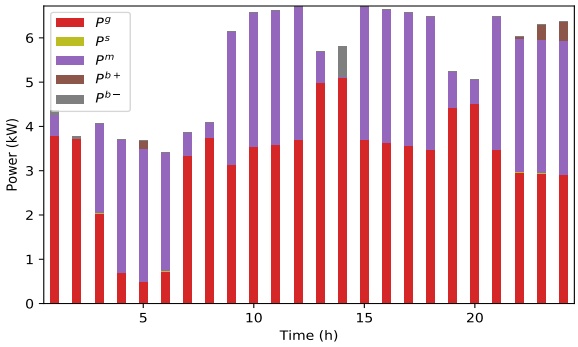

Fig. 11. Islanded microgrid scheduling profile with no PV power output.

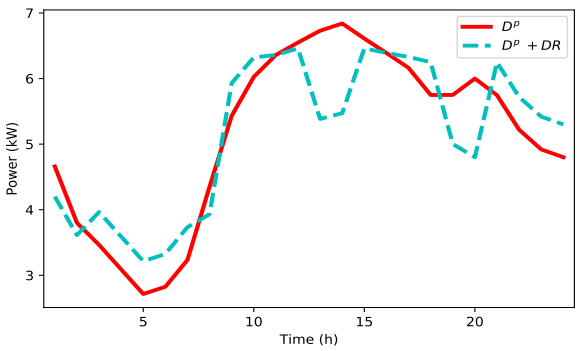

Fig. 12. Active demand with demand response, with no PV power output.

3) Case III: In this case, TT is assumed off–line. Figure 13 shows that the TT is off-line and it is producing no power. Only DG and PV system produce power to meet load demand. PV system does not produce excess power to meet all load demand and charge battery. Hence, battery will not charge or discharge during the 24h scheduling period. Figure 14 shows that the DR shifts responsive load from peak demand to low demand periods to reduce network losses. Moreover, DG will produce lesser power at peak periods.

4) Case IV: In this case, the islanded MG scheduling is studied for 24h period in December. PV system produces lesser power in December at Ouessant island, as shown in Figure 15. It clearly shows that PV system could only produce

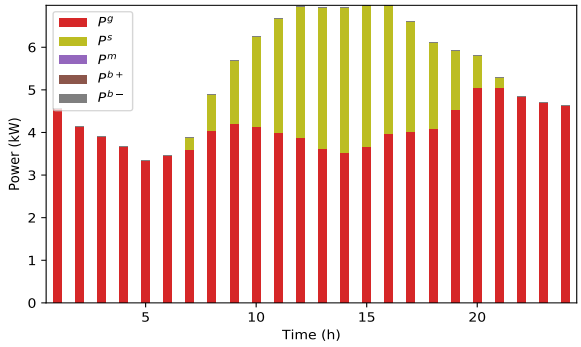

Fig. 13. Islanded microgrid scheduling profile with no tidal power output.

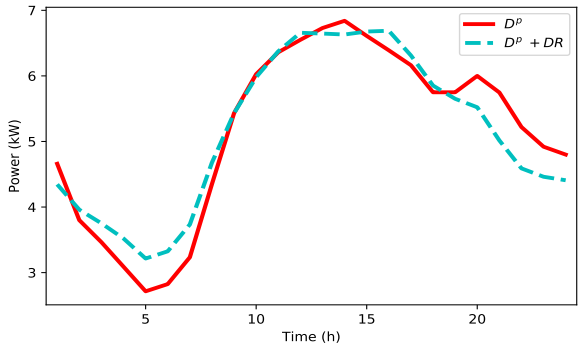

Fig. 14. Active demand with demand response, with no tidal power output.

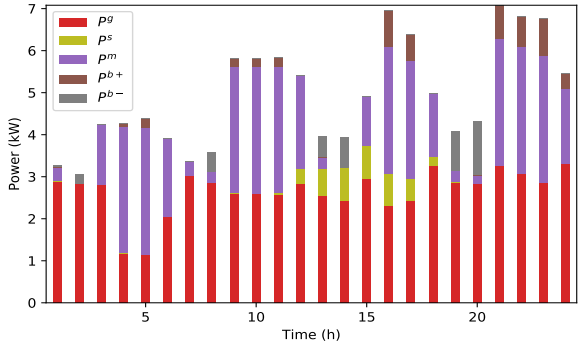

Fig. 15. Islanded microgrid scheduling profile in December.

0093-9994 (c) 2019 IEEE. Personal use is permitted, but republication/redistribution requires IEEE permission. See http://www.ieee.org/publications_standards/publications/rights/index.html for more information.

This article has been accepted for publication in a future issue of this journal, but has not been fully edited. Content may change prior to final publication. Citation information: DOI 10.1109/TIA.2019.2917357, IEEE Transactions on Industry Applications

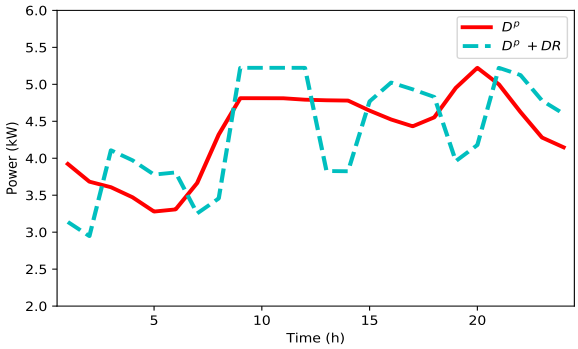

Fig. 16. Active demand with demand response in December.

small amount of power from $t = 11h$ to $t = 18h$. Battery charges at high TT power production periods and discharges when TT and PV system produces less or no power. Figure 16 shows the active power demand profile with and without DR. DR load shifts from peak demand periods. The shifted DR load is recovered at low demand and high TT power output periods. This DR shift reduces network losses and decrease use of DG power production at peak demand periods.

B. Emissions Reduction

In this section, we investigate the reduction in emissions of the islanded MG. It contains DG unit, which produces high GHG emissions against each one kWh unit of electric power production. RESs can be integrated in an islanded MG to reduce DG emission. Therefore, four cases have been considered to study the effects of RESs integration in decreasing the islanded MG emissions. These cases are as follows:

- Case A: DG only.
- Case B: DG, PV, and battery.
- Case C: DG, TT, and battery.
- Case D: DG, PV, TT, and battery.

In case A, DGs have been installed at buses 1, 3, and 6, respectively. All the DGs specifications are similar. In case B, DG, PV system, and battery are installed at buses 1, 3, and 4, respectively. In case C, DG, battery, and TT are installed at buses 1, 4, and 6, respectively. While DG, PV system, battery, and TT are installed at buses 1, 3, 4, and, 6 respectively for case D.

Table IV presents the emissions for each case for 24h period in July. In case A, the islanded MG emissions are $99.45\ kg$. However, they are reduced to $76.68\ kg$ in case B. In cases C and D, the emissions are further reduced to $60.89\ kg$ and $37.35\ kg$, respectively. The ratio of emissions reduction is 22.9 % in case B. While, it is 38.7 % and 62.4 % in cases C and D , respectively. Hence, these case studies clearly prove that RESs and battery can be assumed to play a vital role in reducing emissions in an islanded MG network operation.

TABLE IV
ISLANDED MG EMISSIONS

	Case A	Case B	Case C	Case D
Emissions (kg)	99.45	76.68	60.89	37.35

VI. CONCLUSION

In this paper, a convex energy management system has been developed for an islanded microgrid that optimizes its operating and emission costs. DG operating and emission costs are modeled. Levelized cost of energy models were developed for tidal turbine and PV system. Battery degradation cost was also formulated, which includes temperature and depth of discharge-dependent aging effects. An incentive–based demand response and microgrid network model were also incorporated in the energy management system to facilitate active participation of consumers and satisfy system constraints. The developed second-order cone programming model has achieved the global optimal solution with a lesser optimality gap and reduced computational cost. The simulation results have clearly proved the effectiveness of the proposed model that would aid in optimal scheduling of islanded microgrids in the future.

REFERENCES

[1] M. F. Zia, E. Elbouchikhi, and M. Benbouzid, "Microgrids energy management systems: A critical review on methods, solutions, and prospects," *Applied Energy*, vol. 222, pp. 1033–1055, 2018.
[2] N. Hatziargyriou, Ed., *Microgrids*. John Wiley and Sons Ltd, 2013.
[3] N. L. Diaz, A. C. Luna, J. C. Vasquez, and J. M. Guerrero, "Centralized control architecture for coordination of distributed renewable generation and energy storage in islanded AC microgrids," *IEEE Transactions on Power Electronics*, vol. 32, no. 7, pp. 5202–5213, 2017.
[4] J. G. de Matos, F. S. e Silva, and L. A. d. S. Ribeiro, "Power control in ac isolated microgrids with renewable energy sources and energy storage systems," *IEEE Transactions on Industrial Electronics*, vol. 62, no. 6, pp. 3490–3498, 2015.
[5] J. Huckerby, H. Jeffrey, A. de Andres, and L. Finlay, "An international vision for ocean energy, version–III," Ocean Energy Systems, 2017.
[6] H. Boye, E. Caquot, P. Clement, L. de La Cochetiere, J. Nataf, and P. Sergent, "Rapport de la mission d'étude sur les énergies marines renouvelables," Ministère de l'écologie, du développement durable et de l'énergie, Paris, Tech. Rep., 2013.
[7] D. Magagna and A. Uihlein, "Ocean energy development in europe: Current status and future perspectives," *International Journal of Marine Energy*, vol. 11, pp. 84–104, 2015.
[8] D. Greaves and G. Iglesias, Eds., *Wave and Tidal Energy*. John Wiley & Sons, Ltd, 2018.
[9] A. K. Sleiti, "Tidal power technology review with potential applications in gulf stream," *Renewable and Sustainable Energy Reviews*, vol. 69, pp. 435–441, 2017.
[10] O. H. Mohammed, Y. Amirat, M. Benbouzid, S. Haddad, and G. Feld, "Optimal sizing and energy management of hybrid wind/tidal/PV power generation system for remote areas: Application to the Ouessant French island," in *IECON 2016 - 42nd Annual Conference of the IEEE Industrial Electronics Society*. IEEE, 2016, pp. 4205–4210.
[11] T. El Tawil, J. F. Charpentier, and M. Benbouzid, "Sizing and rough optimization of a hybrid renewable-based farm in a stand-alone marine context," *Renewable Energy*, vol. 115, pp. 1134–1143, 2018.
[12] M. F. Zia, E. Elbouchikhi, and M. Benbouzid, "An energy management system for hybrid energy sources–based stand–alone marine microgrid," in *Proceedings of the 2019 International Conference on Smart Power & Internet Energy Systems*, April 2019, pp. 1–8.
[13] L. Meng, E. R. Sanseverino, A. Luna, T. Dragicevic, J. C. Vasquez, and J. M. Guerrero, "Microgrid supervisory controllers and energy management systems: A literature review," *Renewable and Sustainable Energy Reviews*, vol. 60, pp. 1263–1273, 2016.
[14] F. Cingoz, A. Elrayyah, and Y. Sozer, "Optimized resource management for PV–fuel-cell-based microgrids using load characterizations," *IEEE Transactions on Industry Applications*, vol. 52, no. 2, pp. 1723–1735, 2016.
[15] N. Faridnia, D. Habibi, S. Lachowicz, and A. Kavousifard, "Optimal scheduling in a microgrid with a tidal generation," *Energy*, vol. 171, pp. 435–443, 2019.

0093-9994 (c) 2019 IEEE. Personal use is permitted, but republication/redistribution requires IEEE permission. See http://www.ieee.org/publications_standards/publications/rights/index.html for more information.

This article has been accepted for publication in a future issue of this journal, but has not been fully edited. Content may change prior to final publication. Citation information: DOI 10.1109/TIA.2019.2917357, IEEE Transactions on Industry Applications

[16] S. Sukumar, H. Mokhlis, S. Mekhilef, K. Naidu, and M. Karimi, "Mix-mode energy management strategy and battery sizing for economic operation of grid-tied microgrid," *Energy*, vol. 118, pp. 1322–1333, 2017.

[17] A. C. Luna, N. L. Diaz, M. Graells, J. C. Vasquez, and J. M. Guerrero, "Mixed-integer-linear-programming-based energy management system for hybrid PV-wind-battery microgrids: Modeling, design, and experimental verification," *IEEE Transactions on Power Electronics*, vol. 32, no. 4, pp. 2769–2783, 2017.

[18] N. Anglani, G. Oriti, and M. Colombini, "Optimized energy management system to reduce fuel consumption in remote military microgrids," *IEEE Transactions on Industry Applications*, vol. 53, no. 6, pp. 5777–5785, nov 2017.

[19] F. Conte, F. D'Agostino, P. Pongiglione, M. Saviozzi, and F. Silvestro, "Mixed-integer algorithm for optimal dispatch of integrated PV-storage systems," *IEEE Transactions on Industry Applications*, vol. 55, no. 1, pp. 238–247, 2019.

[20] P. P. Vergara, J. C. López, L. C. da Silva, and M. J. Rider, "Security-constrained optimal energy management system for three-phase residential microgrids," *Electric Power Systems Research*, vol. 146, pp. 371–382, 2017.

[21] B. V. Solanki, K. Bhattacharya, and C. A. Canizares, "A sustainable energy management system for isolated microgrids," *IEEE Transactions on Sustainable Energy*, vol. 8, no. 4, pp. 1507–1517, 2017.

[22] B. V. Solanki, A. Raghurajan, K. Bhattacharya, and C. A. Canizares, "Including smart loads for optimal demand response in integrated energy management systems for isolated microgrids," *IEEE Transactions on Smart Grid*, vol. 8, no. 4, pp. 1739–1748, 2017.

[23] J. S. Giraldo, J. A. Castrillon, and C. A. Castro, "Energy management of isolated microgrids using mixed-integer second-order cone programming," in *2017 IEEE Power & Energy Society General Meeting*. IEEE, 2017, pp. 1–5.

[24] I. Serna-Suárez, G. Ordóñez-Plata, and G. Carrillo-Caicedo, "Microgrid's energy management systems: A survey," in *2015 12th International Conference on the European Energy Market (EEM)*. IEEE, 2015, pp. 1–6.

[25] T. El Tawil, N. Guillou, J. F. Charpentier, and M. Benbouzid, "On tidal current velocity vector time series prediction: A comparative study for a french high tidal energy potential site," *Journal of Marine Science and Engineering*, vol. 7, no. 2, p. 46, 2019.

[26] N. Guillou, S. P. Neill, and P. E. Robins, "Characterising the tidal stream power resource around france using a high-resolution harmonic database," *Renewable Energy*, vol. 123, pp. 706–718, 2018.

[27] N. Guillou, G. Chapalain, and S. P. Neill, "The influence of waves on the tidal kinetic energy resource at a tidal stream energy site," *Applied Energy*, vol. 180, pp. 402–415, 2016.

[28] E. Segura, R. Morales, J. Somolinos, and A. López, "Techno-economic challenges of tidal energy conversion systems: Current status and trends," *Renewable and Sustainable Energy Reviews*, vol. 77, pp. 536–550, 2017.

[29] Z. Zhou, M. Benbouzid, J.-F. Charpentier, F. Scuiller, and T. Tang, "Developments in large marine current turbine technologies – a review," *Renewable and Sustainable Energy Reviews*, vol. 71, pp. 852–858, 2017.

[30] K. Touimi, M. Benbouzid, and P. Tavner, "Tidal stream turbines: With or without a gearbox?" *Ocean Engineering*, vol. 170, pp. 74–88, 2018.

[31] D. Greaves and G. Iglesias, Eds., *Wave and Tidal Energy*. John Wiley & Sons, Ltd, 2018.

[32] M. F. Zia, E. Elbouchikhi, and M. Benbouzid, "Optimal operational planning of scalable DC microgrid with demand response, islanding, and battery degradation cost considerations," *Applied Energy*, vol. 237, pp. 695–707, 2019.

[33] S. Kundu, S. Backhaus, and I. A. Hiskens, "Distributed control of reactive power from photovoltaic inverters," in *2013 IEEE International Symposium on Circuits and Systems (ISCAS2013)*. IEEE, 2013, pp. 249–252.

[34] V. Calderaro, G. Conio, V. Galdi, G. Massa, and A. Piccolo, "Optimal decentralized voltage control for distribution systems with inverter-based distributed generators," *IEEE Transactions on Power Systems*, vol. 29, no. 1, pp. 230–241, 2014.

[35] Q. Nguyen, H. V. Padullaparti, K.-W. Lao, S. Santoso, X. Ke, and N. Samaan, "Exact optimal power dispatch in unbalanced distribution systems with high PV penetration," *IEEE Transactions on Power Systems*, vol. 34, no. 1, pp. 718–728, 2019.

[36] J. A. Taylor, *Convex optimization of power systems*. Cambridge University Press, 2015.

[37] S. Boyd and L. Vandenberghe, *Convex optimization*. Cambridge university press, 2004.

[38] S. H. Low, "Convex relaxation of optimal power flow—part I: Formulations and equivalence," *IEEE Transactions on Control of Network Systems*, vol. 1, no. 1, pp. 15–27, 2014.

[39] S. H. Low, "Convex relaxation of optimal power flow—part II: Exactness," *IEEE Transactions on Control of Network Systems*, vol. 1, no. 2, pp. 177–189, 2014.

[40] C. Coffrin, H. L. Hijazi, and P. Van Hentenryck, "The qc relaxation: A theoretical and computational study on optimal power flow," *IEEE Transactions on Power Systems*, vol. 31, no. 4, pp. 3008–3018, 2016.

[41] B. Kocuk, S. S. Dey, and X. A. Sun, "Strong SOCP relaxations for the optimal power flow problem," *Operations Research*, vol. 64, no. 6, pp. 1177–1196, 2016.

[42] R. Jabr, "Radial distribution load flow using conic programming," *IEEE Transactions on Power Systems*, vol. 21, no. 3, pp. 1458–1459, 2006.

[43] S. Sojoudi and J. Lavaei, "Physics of power networks makes hard optimization problems easy to solve," in *2012 IEEE Power and Energy Society General Meeting*. IEEE, 2012, pp. 1–8.

[44] L. Gurobi Optimization, "Gurobi optimizer reference manual," 2018. [Online]. Available: http://www.gurobi.com

[45] A. Wächter and L. T. Biegler, "On the implementation of an interior-point filter line-search algorithm for large-scale nonlinear programming," *Mathematical Programming*, vol. 106, no. 1, pp. 25–57, 2005.

[46] L. Beal, D. Hill, R. Martin, and J. Hedengren, "Gekko optimization suite," *Processes*, vol. 6, no. 8, p. 106, 2018.

[47] N. Pogaku, M. Prodanovic, and T. C. Green, "Modeling, analysis and testing of autonomous operation of an inverter-based microgrid," *IEEE Transactions on Power Electronics*, vol. 22, no. 2, pp. 613–625, 2007.

[48] C. Li, S. K. Chaudhary, M. Savaghebi, J. C. Vasquez, and J. M. Guerrero, "Power flow analysis for low-voltage AC and DC microgrids considering droop control and virtual impedance," *IEEE Transactions on Smart Grid*, vol. 8, no. 6, pp. 2754–2764, 2017.

Muhammad Fahad Zia (S'18) received the BS degree in Electrical Engineering with honours from University of Engineering and Technology, Lahore, Pakistan, in 2009, and MS in Electrical Engineering from King Fahd Univeristy of Petroleum and Minerals, Dhahran, Saudi Arabia in 2014. He served as an Assistant Manager (Operations) at PTCL, Lahore, Pakistan from 2009-2010. From 2010-2012, he served as a Lab Engineer and from 2014-2017, he served as Lecturer and Assistant Professor at University of Management and Technology, Lahore, Pakistan.

Currently, he is a PhD candidate in Electrical Engineering at University of Brest, Brest, France. His main research interests and experience include AC/DC microgrids, marine microgrids, energy management system, power electronics, distributed generation and storage, transactive energy, and its applications in microgrids.

Elhoussin Elbouchikhi (S'12, M'18, SM'19) received the diploma engineer degree (Dipl.-Ing.) in Automatic and Electrical Engineering and Research Master's degree in Automatic Systems, Computer Science and Decision, from the National Polytechnic Institute of Toulouse (INP-ENSEEIHT), Toulouse, France, in 2010, and the Ph.D degree in Electrical Engineering in 2013 from the University of Brest, Brest, France.

After receiving the Ph.D. degree, he has been a Post-Doctoral Researcher at ISEN Brest, Yncréa Ouest, Brest, France and an Associate Member of the LBMS Laboratory (EA 4325) from October 2013 to September 2014. Since September 2014, he is an Associate Professor at ISEN Brest, Yncréa Ouest, Brest, France and is a member of the Institut de Recherche Dupuy de Lôme - IRDL (UMR CNRS 6027). Dr. ELBOUCHIKHI is an IEEE Senior Member. His main current research interests and experience include electrical machines control and faults detection and diagnosis, fault tolerant control in marine current turbines, and signal processing and statistics for power systems monitoring. He is also interested in energy management systems in microgrids and renewable energy applications such as marine currents turbines, wind turbines, and hybrid generation systems.

0093-9994 (c) 2019 IEEE. Personal use is permitted, but republication/redistribution requires IEEE permission. See http://www.ieee.org/publications_standards/publications/rights/index.html for more information.

This article has been accepted for publication in a future issue of this journal, but has not been fully edited. Content may change prior to final publication. Citation information: DOI 10.1109/TIA.2019.2917357, IEEE Transactions on Industry Applications

Mohamed Benbouzid (S'92–M'95–SM'98) received the B.Sc. degree in electrical engineering from the University of Batna, Batna, Algeria, in 1990, the M.Sc. and Ph.D. degrees in electrical and computer engineering from the National Polytechnic Institute of Grenoble, Grenoble, France, in 1991 and 1994, respectively, and the Habilitation à Diriger des Recherches degree from the University of Picardie "Jules Verne," Amiens, France, in 2000.

After receiving the Ph.D. degree, he joined the Professional Institute of Amiens, University of Picardie "Jules Verne," where he was an Associate Professor of electrical and computer engineering. Since September 2004, he has been with the University of Brest, Brest, France, where he is a Full Professor of electrical engineering. Prof. Benbouzid is also a Distinguished Professor and a 1000 Talent Expert at the Shanghai Maritime University, Shanghai, China. His main research interests and experience include analysis, design, and control of electric machines, variable-speed drives for traction, propulsion, and renewable energy applications, and fault diagnosis of electric machines.

Prof. Benbouzid is a Fellow of the IET and an IEEE Senior Member. He is the Editor-in-Chief of the International Journal on Energy Conversion. He is also an Associate Editor of the IEEE Transactions on Energy Conversion and the IEEE Transactions on Vehicular Technology. He is a Subject Editor for the IET Renewable Power Generation.

Josep M. Guerrero (S'01-M'04-SM'08-FM'15) received the B.S. degree in telecommunications engineering, the M.S. degree in electronics engineering, and the Ph.D. degree in power electronics from the Technical University of Catalonia, Barcelona, in 1997, 2000 and 2003, respectively. Since 2011, he has been a Full Professor with the Department of Energy Technology, Aalborg University, Denmark, where he is responsible for the Microgrid Research Program (www.microgrids.et.aau.dk). From 2014 he is chair Professor in Shandong University; from 2015 he is a distinguished guest Professor in Hunan University; and from 2016 he is a visiting professor fellow at Aston University, UK, and a guest Professor at the Nanjing University of Posts and Telecommunications. From 2019 he became a Villum Investigator.

His research interests are oriented to different microgrid aspects, including power electronics, distributed energy-storage systems, hierarchical and cooperative control, energy management systems, smart metering and the internet of things for AC/DC microgrid clusters and islanded minigrids; recently specially focused on maritime microgrids for electrical ships, vessels, ferries and seaports. Prof. Guerrero is an Associate Editor for a number of IEEE TRANSACTIONS. He has published more than 500 journal papers in the fields of microgrids and renewable energy systems, which are cited more than 30,000 times. He received the best paper award of the IEEE Transactions on Energy Conversion for the period 2014-2015, and the best paper prize of IEEE-PES in 2015. As well, he received the best paper award of the Journal of Power Electronics in 2016. During five consecutive years, from 2014 to 2018, he was awarded by Clarivate Analytics (former Thomson Reuters) as Highly Cited Researcher. In 2015 he was elevated as IEEE Fellow for his contributions on "distributed power systems and microgrids".

0093-9994 (c) 2019 IEEE. Personal use is permitted, but republication/redistribution requires IEEE permission. See http://www.ieee.org/publications_standards/publications/rights/index.html for more information.